PHILOSOPHICAL TRANSACTIONS OF THE ROYAL SOCIETY A

Phil. Trans. R. Soc. A (2010) **368**, 4389–4405
doi:10.1098/rsta.2010.0123

Core–shell $La_{1-x}Sr_xMnO_3$ nanoparticles as colloidal mediators for magnetic fluid hyperthermia

By E. Pollert[1,*], O. Kaman[1,2], P. Veverka[1], M. Veverka[1], M. Maryško[1], K. Závěta[1], M. Kačenka[1,2], I. Lukeš[2], P. Jendelová[3], P. Kašpar[4], M. Burian[5] and V. Herynek[5]

[1]*Institute of Physics, Academy of Sciences of the Czech Republic, v.v.i., Cukrovarnická 10, 162 53 Prague 6, Czech Republic*
[2]*Faculty of Science, Charles University, Hlavova 8, 128 40 Prague 2, Czech Republic*
[3]*Institute of Experimental Medicine, Academy of Sciences of the Czech Republic, v.v.i., Vídeňská 1083, 142 40 Prague 4, Czech Republic*
[4]*Faculty of Electrical Engineering, Czech Technical University, Technická 2, 166 27 Prague 6, Czech Republic*
[5]*Institute for Clinical and Experimental Medicine, Vídeňská 1958, 140 21 Prague 4, Czech Republic*

Core–shell nanoparticles consisting of $La_{0.75}Sr_{0.25}MnO_3$ cores covered by silica were synthesized by a procedure consisting of several steps, including the sol–gel method in the presence of citric acid and ethylene glycol, thermal and mechanical treatment, encapsulation employing tetraethoxysilane and final separation by centrifugation in order to get the required size fraction. Morphological studies revealed well-separated particles that form a stable water suspension. Magnetic studies include magnetization measurements and investigation of the ferromagnetic–superparamagnetic–paramagnetic transition. Magnetic heating experiments in 'calorimetric mode' were used to determine the heating efficiency of the particles in water suspension and further employed for biological studies of extracellular and intracellular effects analysed by tests of viability.

Keywords: magnetic fluid hyperthermia; manganese perovskites; nanoparticles

1. Introduction

There is continuing interest in magnetic fluid hyperthermia as a complementary oncological treatment. Various aspects of the method have been widely discussed in a number of articles, e.g. Andrä (1998), Hergt *et al.* (2002), Kallumadil *et al.* (2009), Mornet *et al.* (2004, 2006) and Pankhurst *et al.* (2003, 2009). The concept of the treatment is based on the higher heat sensitivity of tumour cells in comparison with healthy tissue. So, exposing the tissue to temperatures

*Author for correspondence (pollert@fzu.cz).

One contribution of 14 to a Theme Issue 'Nanoparticles'.

between 42 and 45°C leads to destruction of the tumour cells and sparing of the healthy ones. The heating is effected essentially by magnetic losses, and two kinds of magnetic cores should thus be distinguished: superparamagnetic particles, where the loss mechanism results from the rotation of magnetic moments, and ferro- or ferrimagnetic particles, where heating is a consequence of hysteresis losses. In addition, frictional losses due to rotational Brownian motion in the carrier liquid can contribute to the total effect.

Some restrictions should be considered with respect to the applied alternating magnetic field. First, for technical reasons, there is a limit on the amplitude of the applied field to about 8–16 $\mathrm{kA\,m^{-1}}$ (Jordan *et al.* 2001). Further, attention should be paid to the applied frequency, which is required to be higher than 50 kHz to avoid neuromuscular electrostimulation but lower than 10 MHz to achieve a satisfactory penetration depth of the radiofrequency field into the electrically conducting tissue (Hill 1985). Therefore, it is evident that, besides the modulation of the parameters of the applied alternating magnetic field, a suitable adjustment of the core's properties is important. This concerns magnetization and coercivity, thus providing a reasonable heating efficiency and a Curie temperature that should be adjusted slightly above the therapeutic temperature (approx. 45°C) in order to achieve a self-controlled heating mechanism. One possible approach to solve the outlined task is the use of complex magnetic oxides as core materials, whose magnetic properties can be properly tailored in various ways, such as modification of the intrinsic properties depending on the composition and structure, or modification of the extrinsic properties (e.g. particle size) depending on the synthesis procedure and alternatively employing multiphase materials. These possibilities were discussed with several examples in our recent paper (Pollert *et al.* 2009), where the position of $La_{1-x}Sr_xMnO_3$ (LSMO) perovskites, offering exceptional feasibility, was stressed. Simultaneously, attention should be paid to the quality of the coating, ensuring stability of the suspension and biocompatibility, indispensable properties with respect to potential medical applications.

2. Synthesis

Synthesis of LSMO nanoparticle cores consists of the following steps. Preparation of the precursor via the sol–gel method employing citric acid (AC) and ethylene glycol (EG), accompanied by subsequent evaporation of water, drying and calcination by the procedure reported previously (Vasseur *et al.* 2006), but suitably modified with respect to the acid–base equilibria.

A distinctive feature of this step is the formation of citric–metal complexes and simultaneous polyesterification between them or redundant AC and EG. The process widely studied in detail is described in Kakihana & Yoshimura (1999). Employing a simplified approach, it is evident that increasing basicity in the sequence

$$\mathrm{AC} + \mathrm{H_2O} \rightarrow \mathrm{AC^-} + \mathrm{H_3O^+} \tag{2.1}$$

$$\mathrm{AC^-} + \mathrm{H_2O} \rightarrow \mathrm{AC^{2-}} + \mathrm{H_3O^+} \tag{2.2}$$

$$\mathrm{AC^{2-}} + \mathrm{H_2O} \rightarrow \mathrm{AC^{3-}} + \mathrm{H_3O^+} \tag{2.3}$$

Table 1. Estimated dissociation equilibria of citric acid in sols A and B.

sol	pH	AC^- (mol%)	AC^{2-} (mol%)	AC^{3-} (mol%)
A	7.2[a]		20	80
	6.8[b]	1	37	62
B	8.3[a]		2.5	97.5
	7.8[b]		6	94

[a]Starting values at 25°C.
[b]Final values at 80–90°C.

favours the formation of the metal complexes. On the other hand, esterification, an example of a possible primary reaction step given below, occurs preferentially at low pH, and is inhibited at higher pH:

$$\begin{array}{l} \mathrm{CH_2{-}COOH} \\ | \\ \mathrm{HO{-}C{-}COOH} \\ | \\ \mathrm{CH_2{-}COOH} \end{array} + \mathrm{HO{-}CH_2CH_2{-}OH} \rightarrow \begin{array}{l} \mathrm{CH_2{-}COOH} \\ | \\ \mathrm{HO{-}C{-}CO{-}O{-}CH_2CH_2{-}OH} \\ | \\ \mathrm{CH_2{-}COOH} \end{array} + \mathrm{H_2O} \tag{2.4}$$

The resulting ester still comprises carboxylic and alcoholic groups, allowing a subsequent linking that leads to a cross-linked structure. Metal species as well as complexes thus become stabilized in the polyester network, segregation of the metals ions is suppressed and compositional homogeneity is achieved.

Therefore, the solution of the cationic components, AC and EG in the ratio of $(1-x)[La^{3+}]/x[Sr^{2+}]/[Mn^{2+}]/1.5[AC]/2.25[EG]$, e.g. $x=0.25$, were mixed together and ammonium hydroxide was added to adjust the value of the pH. Then, the sols were subjected to slow heating up to 80–90°C under continuous stirring, followed by drying at 160°C and calcination at 400°C in air.

In order to elucidate, at least qualitatively, the problem already outlined above and exemplified by the formation of $BaTi_4O_9$ (Kakihana & Yoshimura 1999), the influence of the pH value on the phase composition of the prepared precursors was tested. The attainable data of citric acid dissociation measured on the binary water–methanol system (Papanastasiou & Ziogas 1989) were employed for a rough estimate of the corresponding equilibria in our study (table 1). It seems to be obvious that, for sol A, the esterification reactions can occur, but at pH 8.3 it is suppressed.

The resulting effect can be understood from the comparison of the X-ray phase analysis of the precursors calcinated at 400°C, shown in figures 1 and 2. Pyrolysis of the polyester matrix containing homogeneously dispersed immobilized cations in sample A resulted in a precursor possessing typically an amorphous structure, and only the growth of the perovskite phase was detected. In contrast, citric acid in the sol of sample B is almost completely dissociated, and the formation of the polyester network stabilizing the homogeneous distribution of cations is hindered. Therefore, in addition to the perovskite phase, various other phases

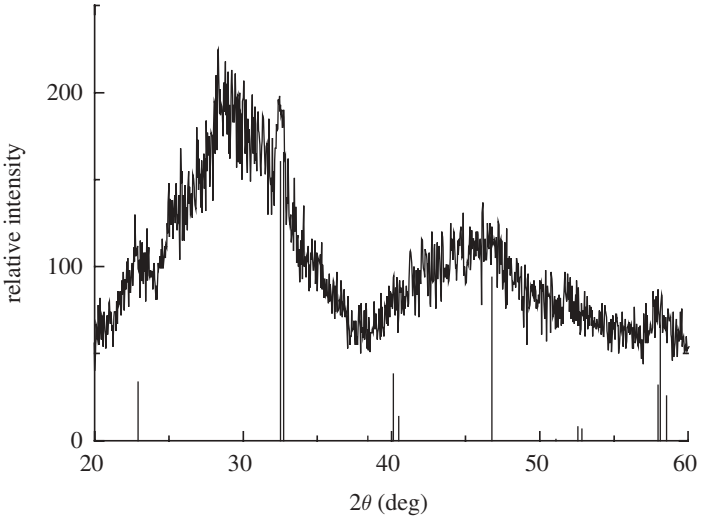

Figure 1. X-ray phase analysis of the precursor prepared from sol A. Thin solid lines, manganese perovskite phase.

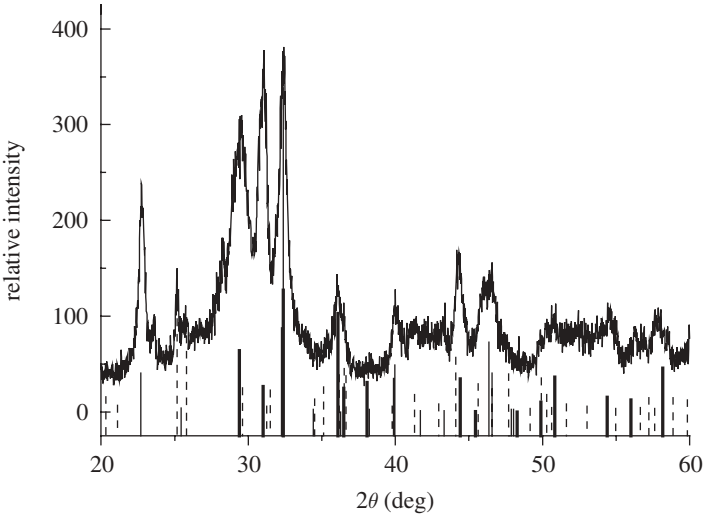

Figure 2. X-ray phase analysis of the precursor prepared from sol B. Thin solid lines, manganese perovskite phase; thick solid lines, Mn_3O_4; dashed lines, $SrCO_3$.

may crystallize. Particularly, this is the case for hausmannite, Mn_3O_4 which can be hardly dissolved by annealing at the moderate temperatures needed for the growth of nanoparticles of a size smaller than 100 nm.

Annealing of the precursor in air at temperatures in the range of 650–900°C for a limited time of 3 h gives rise to single-phase manganese perovskite crystallites with mean size gradually increasing with temperature from 20 to 120 nm.

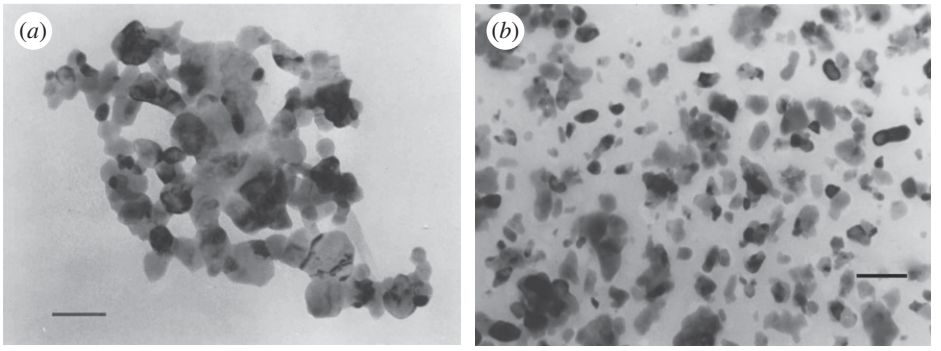

Figure 3. (*a*) Fresh annealed sample, grains connected by 'bridges' and (*b*) separated grains after mechanical treatment by rolling and milling. Scale bars, (*a*,*b*) 100 nm.

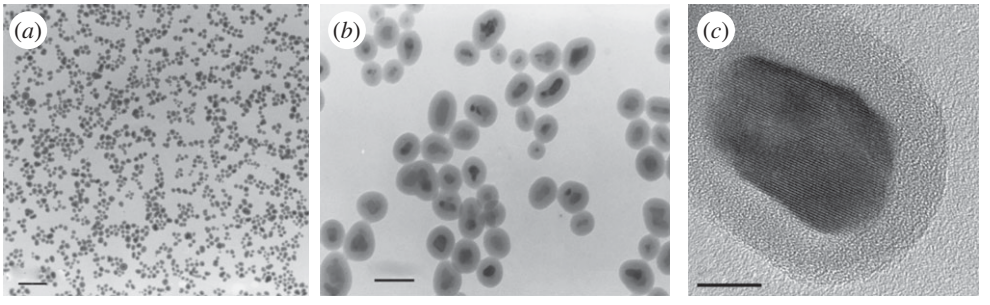

Figure 4. An example of the encapsulated LSMO(0.25)–SiO_2; transmission and high-resolution electron micrographs. Scale bars, (*a*) 400 nm, (*b*) 100 nm and (*c*) 10 nm.

Mechanical treatment by rolling and milling in order to destroy the 'connecting bridges' between the individual grains, arising due to a tendency to sintering, and to separate the individual grains from the agglomerates, is shown in figure 3*a*,*b*.

Magnetic cores were covered by a continuous layer of hydrated silica oxide, which, due to electrostatic repulsions of the $(Si–O)^-$ groups present on the surface, generates suspensions of high stability in a water medium of pH approximately 7. Simultaneously, the silica shell should form a biologically inert barrier, protecting the surrounding environment from the chemical effects of the core. Therefore, this represents a basic implementation that would probably allow application by direct injection.

The encapsulation procedure is described in detail elsewhere (Kaman *et al.* 2009). It consists of the treatment of the surface of the synthesized grains by nitric acid, subsequent stabilization of the suspension by ammonium citrate and coating by hydrated silica oxide in a medium of water, ethanol and ammonia at 40°C, employing tetraethoxysilane. Finally, in order to get nanoparticles of the required size, the product was subjected to a separation procedure via centrifugation. Typical electron micrographs for $La_{0.75}Sr_{0.25}MnO_3$ (denoted LSMO(0.25)) are shown in figure 4.

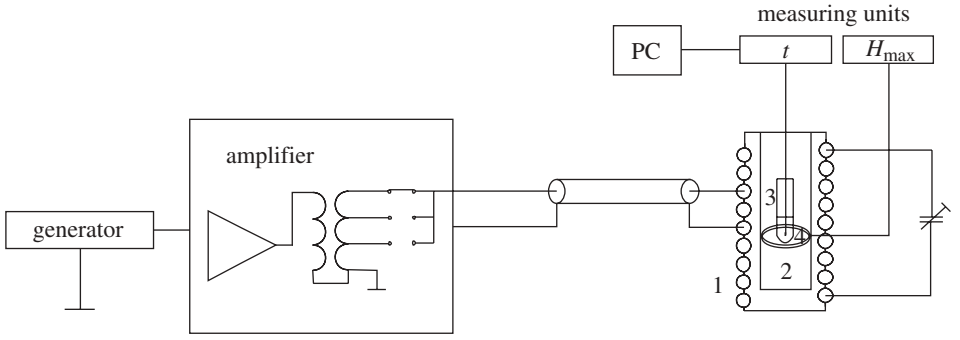

Figure 5. Scheme of the apparatus for magnetic heating experiments: 1, water-cooled exciting coil; 2, insulating polystyrene foam; 3, plastic tube; 4, search coil.

Table 2. Alternating field parameters applicable for the apparatus.

ν (kHz)	H_{max} (kA m^{-1})
960	3.2–6
480	3.2–8.8
107	6–13.7

3. Characterization methods

The phase composition of the samples and the mean size of the particles were determined by X-ray powder diffraction with a Bruker D8 diffractometer using the Cu Kα line and a Sol-X energy-dispersive detector. X-ray diffraction (XRD) patterns were analysed by the Rietveld method with the help of the FULLPROF program. The crystallite size delimits the XRD coherence length and thus contributes to the peak width. A Thompson–Cox–Hastings pseudo-Voigt profile was used to resolve the instrumental, strain and size contributions to peak broadening. Instrumental resolution was determined by measuring strain-free tungsten powder with a crystallite size of 9.4 µm. The sizes and shapes of the particles were also directly observed by transmission electron microscopy (Philips EM 201).

The content of manganese both in the suspension and in powder samples was determined photometrically at a wavelength of 526 nm. The manganese ions were oxidized to permanganate and absorption spectra were measured with a spectrophotometer (Unicam UV300).

Static magnetic properties were measured by means of a SQUID (superconducting quantum interference device) magnetometer (MPMS-5S by Quantum Design) in fields up to 2 T and in the temperature range of 5–370 K.

Magnetic heating experiments in 'calorimetric mode' were performed on a 'home-made' apparatus (figure 5) under alternating fields with the parameters listed in table 2. The measured suspensions in plastic tubes (length 95 mm, diameter 14 mm), thermally insulated by polystyrene foam, were placed into an exciting coil of inner diameter 80 mm in the position of the search coil.

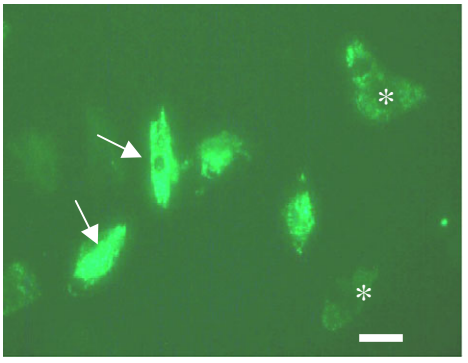

Figure 6. Stem cells (rMSCs) growing in culture after incubation with LSMO(0.25)–(SiO_2–NH_2–fluorescein–SiO_2) nanoparticles. Scale bar, 20 µm.

As a model for testing the suitability of LSMO(0.25)–SiO_2 nanoparticle suspensions for cell internalization, we have chosen adult rat mesenchymal stem cells (rMSCs), since they are easily derived from the bone marrow, can migrate towards tumours and can be used in gene therapy as carriers for therapeutic genes. In addition, they can be easily harvested and expanded *in vitro*. The cells were isolated from rat femur bones as described elsewhere (Azizi *et al.* 1998). Cells from passages 2–5 were labelled by adding a suspension of nanoparticles at a concentration of 6.0 $mg_{Mn}\,l^{-1}$ to the cultivation media for 48 h. At the end of the labelling experiment, the cells were harvested and counted in a Bûrker chamber. Viability was determined using the trypan blue exclusion test, which can determine the number of viable cells present in a cell suspension. The test is based on the principle that live cells possess intact cell membranes that exclude certain dyes, such as trypan blue, whereas dead cells do not (Carvalho *et al.* 2008). Cell viabilities before the heating experiments, immediately after and the next day were determined analogously.

The *in vitro* magnetic heating experiments were carried out in the apparatus described above using a cell–nanoparticle suspension. In experiments studying the internalization of nanoparticles, the cells were labelled prior to the experiment. The presence of nanoparticles inside the cells in the case of nanoparticles containing fluorescein was detected by fluorescent microscopy (for an example, see figure 6); details are reported elsewhere (Kačenka *et al.* submitted). In figure 6, it can be seen that the particles are not distributed uniformly; according to the intensity of the fluorescent staining, some cells are labelled more (arrows) and some less (asterisks).

Magnetic resonance relaxivity measurements carried out on a 0.5 T Bruker Minispec MQ20 relaxometer at 295 K were used to determine semiquantitatively the contents of manganese inside the cells. Identical protocols were employed to find the T_2 values of both the nanoparticles and the cell suspensions. The contributions of the liquid media were negligible and therefore disregarded.

The values determined for the nanoparticle suspensions were converted to relaxation rates and related to the Mn concentration according to the following formula to obtain the relaxivity value r_2:

$$r_2\,(s^{-1}\,mmol^{-1}) = T_2^{-1}\,c^{-1}. \tag{3.1}$$

Table 3. Estimated content of Mn inside the cells.

sample	$r_2^{22^\circ C}$ (nanoparticle suspensions) ($s^{-1}\,mmol^{-1}$)	Mn/cell (pg/cell)
LSMO(0.25)–SiO_2	617 ± 22	0.17
LSMO(0.25)–(SiO_2–NH_2–fluorescein–SiO_2)	490 ± 50	0.18

Table 4. Fundamental data of the uncoated $La_{0.75}Sr_{0.25}MnO_3$, denoted as LSMO(0.25), and coated $La_{0.75}Sr_{0.25}MnO_3$, denoted as LSMO(0.25)–SiO_2. Here c_{Mn} is the content of manganese ions in uncoated particles, coated particles and particle suspension.

sample	c_{Mn} (wt%)	d_{XRD} (nm)	T_c^a (K)	$M^b_{750\,kA\,m^{-1}}$ ($A\,m^2\,kg^{-1}_{LSMO}$)	H_c^b ($kA\,m^{-1}$)
LSMO(0.25) dry	23.96[c]	20	336	24	1.1
LSMO(0.25)–SiO_2 dry	6.9[d]	24	335	31	0.5
LSMO(0.25)–SiO_2 suspension	0.35[d]			33	

[a]From the Arrot plot relation $H/M = a(T - T_c) + bM^2$ (Arrot 1957).
[b]At 300 K.
[c]Original synthesized composition.
[d]Determined by chemical analysis.

Then, employing the relaxation time measurements done on cell suspensions, the average content of Mn inside the cells was estimated. The respective data are given in table 3.

4. Magnetic properties

Whereas the parent compound $LaMnO_3$ is an antiferromagnetic insulator, the substitution of lanthanum for strontium ions markedly changes its behaviour. It leads to a gradual decrease in steric distortion and variation in the valencies of manganese, formally described as $La^{3+} + Mn^{3+} \rightarrow Sr^{2+} + Mn^{4+}$. Consequently, due to double-exchange interactions, ferromagnetic ordering arises accompanied by an insulator–metal transition (Asamitsu *et al.* 1996). Simultaneously, the resulting properties are markedly influenced by the decrease in the crystallite size, typically below approximately 100 nm. This leads to a gradual diminution in the stability of the magnetic ordering because of an increasing influence of the outer magnetically 'dead layer' (Vasseur *et al.* 2006; Jirák *et al.* 2010).

Therefore, the properties of the LSMO cores can be tailored by both variation of the composition and modification of the particle size depending on the synthesis procedure. Fundamental data of the samples selected for the present study are summarized in table 4.

The room-temperature magnetization curves exhibit very small hysteresis and a lack of saturation even at 1600 $kA\,m^{-1}$, which indicates that the particles in the studied samples may occur predominantly in the superparamagnetic state.

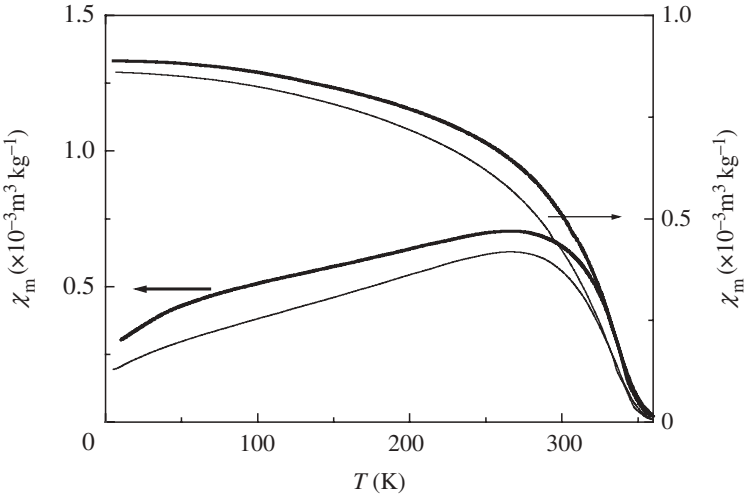

Figure 7. Temperature dependences of the mass susceptibility of the $La_{0.75}Sr_{0.25}MnO_3$ core in the zero-field-cooled (ZFC) and field-cooled (FC) states. Thick line, LSMO(0.25); thin line, LSMO(0.25)–SiO_2 dry.

A better insight into the ferromagnetic–superparamagnetic transition in the studied system is given by the temperature dependences of susceptibilities χ_{ZFC} and χ_{FC} after cooling in zero magnetic field (ZFC) and cooling in magnetic field (FC), respectively (figure 7), measured with the aim of determining the distribution of blocking temperatures (T_B). It is evident that systems possessing a distribution of particle sizes should also exhibit a corresponding distribution p of blocking temperatures, proportional, as shown in Lu *et al.* (2000), to the T derivative of the difference between χ_{ZFC} and χ_{FC}:

$$p(T_B) = \frac{d(\chi_{ZFC} - \chi_{FC})}{dT}. \tag{4.1}$$

The evaluated dependences of the blocking temperatures depicted in figure 8 show values of $T_{Bmax} = 260\,K$ for the LSMO(0.25) sample and $T_{Bmax} = 285\,K$ for the LSMO(0.25)–SiO_2 dry sample.

We may thus expect that, in the temperature range of interest (300–350 K), particles in both blocked and superparamagnetic states will be present. In order to test this possibility, the magnetization curves for the sample LSMO(0.25)–SiO_2 dry were plotted against H/T in the temperature range of 300–350 K in figure 9. The curves for various temperatures do not merge into a unified dependence, as would be expected for a system of superparamagnetic particles with negligible interactions, but display a distinct shift to lower values with increased temperatures, essentially preserving their characteristic shapes. This behaviour points to the expected simultaneous presence of ferromagnetic particles with marked dependence of their moments on temperature close to T_c, and superparamagnetic ones not saturated even at the highest magnetic fields used.

The measurements, however, were done in a quasi-static regime of the time window of approximately 1 s, while the heating efficiency experiments, discussed subsequently, correspond to a time window in the range of approximately

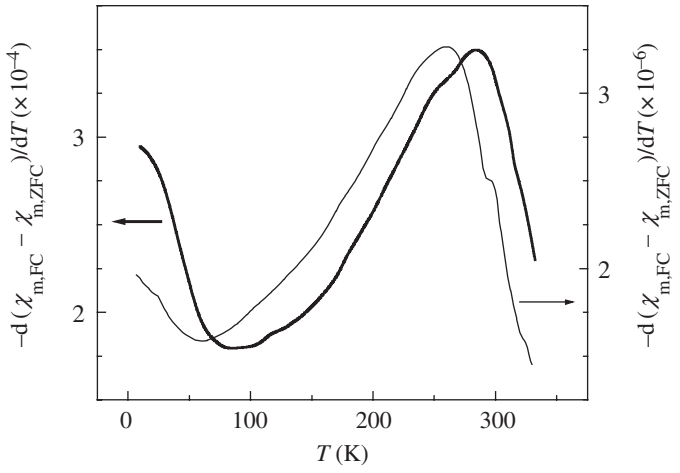

Figure 8. Distributions of the blocking temperatures T_{B} derived from $\chi_{\mathrm{ZFC}}(T)$ and $\chi_{\mathrm{FC}}(T)$. Thick line, LSMO(0.25); thin line, LSMO(0.25)–SiO_2 dry.

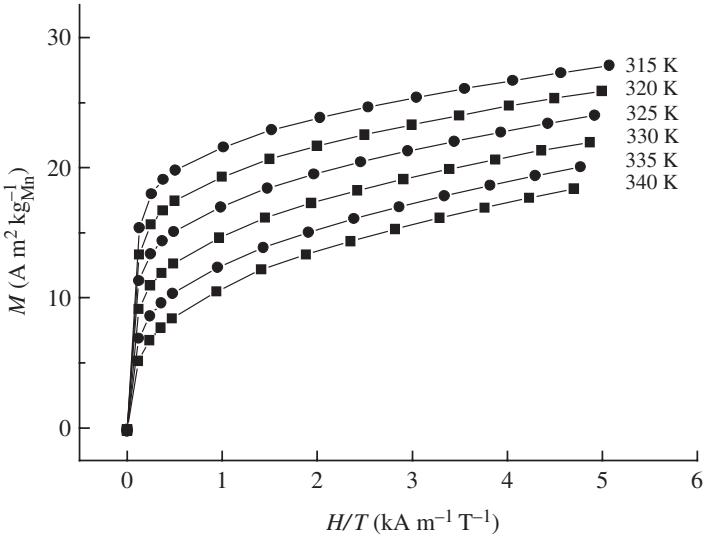

Figure 9. Specific magnetic moment of LSMO(0.25)–SiO_2 dry plotted against H/T.

10^{-5}–10^{-6} s, thus markedly influencing the transition of these nanoparticles from the blocked to the superparamagnetic state (Néel 1949). Our recent comparative experiments carried out on maghemite nanoparticles of mean size $d_{\mathrm{XRD}} \sim 5$ nm made via measurements of DC magnetic properties and Mössbauer spectroscopy with rather different time windows, about 1 s for the former and 10^{-7} s for the latter, confirmed this effect, i.e. shift of the blocking temperatures to several times higher temperatures (Závěta *et al.* 2006). Therefore, an analogous behaviour, i.e. predominant ferromagnetic behaviour for the applied frequencies, can be supposed at the temperatures used in the actually studied samples.

5. Magnetic heating

The basic contribution to the heating effect corresponds to the magnetic losses P ($\mathrm{W\,g_x^{-1}}$) given by the relation

$$P = \frac{\mu_0 \nu}{w_{\mathrm{Mn}}} \oint_H M \,\mathrm{d}H, \tag{5.1}$$

where μ_0 is the vacuum permeability, ν the frequency of the alternating field (Hz), w the weight fraction of magnetic elements x (Mn), H the magnetic field ($\mathrm{kA\,m^{-1}}$) and M the magnetization of the measured sample ($\mathrm{A\,m^2\,kg_x^{-1}}$). The apparent linear dependence of the power loss on the frequency following from equation (5.1) may be basically influenced by changes in the parameters of the hysteresis loop with both frequency and temperature.

In principle, direct measurements of the AC hysteresis loops, where the corresponding area of the hysteresis loop relates to the power losses, can be used for the determination of the power input (Pollert *et al.* 2007). Nevertheless, the use of 'calorimetric' experiments carried out with magnetic particles in a liquid medium appears to be more reasonable because the conditions are closer to the intended application as they also include the heat flow to the surroundings. Further, such an experiment can also reflect additional influences like frictional losses on the one hand and the negative effect of a tendency to agglomerate on the other (Kaman *et al.* 2009).

Here, the observed variable is the temperature, and its typical dependence on the time of exposure to the radiofrequency field of $H_{\max} = 6.05\,\mathrm{kA\,m^{-1}}$, $\nu = 960$, 480 and 107 kHz, is illustrated in figure 10. The rapid increase in the temperature for an applied frequency of 960 kHz saturates at the maximum achieved temperature of $T_{\max} = 64^{\circ}\mathrm{C}$ in rough correspondence with the determined Curie temperature (table 4). In contrast, there are less steep dependences at lower frequencies, particularly 107 kHz. The reason lies in the decrease of the magnetic hysteresis losses and equilibrium with the thermal losses thus occurs at lower temperatures.

Heating efficiency is currently characterized by the specific absorption rate (SAR) defined as

$$\mathrm{SAR} = \frac{C}{w_x}\frac{\mathrm{d}T}{\mathrm{d}t}, \tag{5.2}$$

where C is the specific heat of the medium in which the particles are suspended (usually roughly equal to the specific heat of water, i.e. $4.18\,\mathrm{J\,g^{-1}}$), $\mathrm{d}T/\mathrm{d}t$ is the slope of the temperature versus time curve and w_x is the weight fraction of magnetic elements x in the medium. The specific absorption rate depends on the applied parameters of the alternating field, as can be understood from the power dissipation term (Rosensweig 2002)

$$P = \mu_0 \pi \chi'' \nu H^2, \tag{5.3}$$

where μ_0 is the permeability of free space, χ'' the imaginary component of the susceptibility, generally a function of frequency, ν the frequency and H the applied field strength. It was predicted (Rosensweig 2002) and recently confirmed (Kallumadil *et al.* 2009) that for the frequencies used in hyperthermia

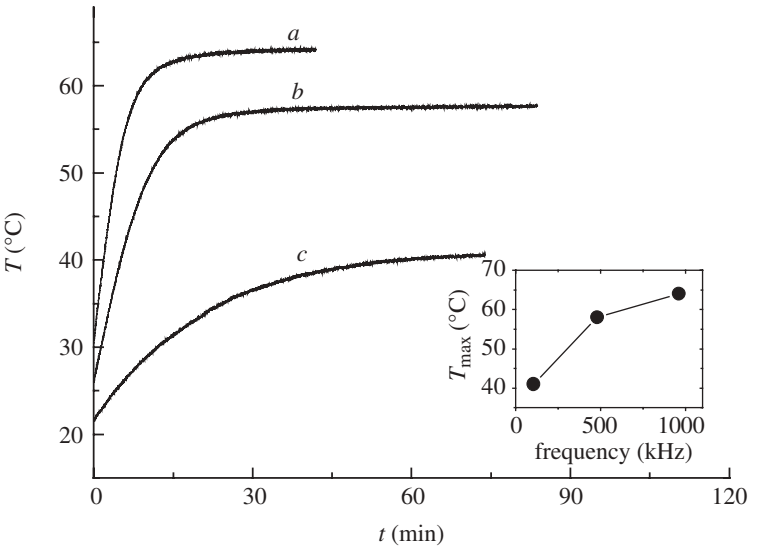

Figure 10. Magnetic heating of the LSMO(0.25)–SiO_2 aqueous suspension, under applied alternating field, $H_{max} = 6.05\,kA\,m^{-1}$, at (*a*) $\nu = 960\,kHz$, (*b*) 480 kHz and (*c*) 107 kHz. Inset—dependence of the achieved T_{max} on the applied frequency.

experiments, i.e. 100 kHz to 1 MHz, and for polydisperse samples, χ'' is frequency-independent. An analogous situation exists in our magnetic suspension, as can be seen from the inset in figure 11, with a certain amount of caution because of the limited number of experimental data.

This therefore offers the potential to plot the function $SAR = f(\nu H^2)$ in order to demonstrate the evolution of the SAR values of LSMO(0.25)–SiO_2 suspension with applied H_{max} and frequency (figure 11).

Let us note that, for 960 kHz, the amplitude $H_{max} = 6.05\,kA\,m^{-1}$ and, for 480 kHz, $H_{max} = 8.7\,kA\,m^{-1}$ are the highest accessible fields in the present experimental arrangement. The highest SAR value of $30\,W\,g_{Mn}^{-1}$ was thus reached for the applied $H_{max} = 8.7\,kA\,m^{-1}$ and $\nu = 480\,kHz$.

6. Preliminary magnetic heating examinations *in vitro*

There are two types of heating that should be distinguished, namely extracellular, by nanoparticles surrounding the cells, and intracellular, by internalized nanoparticles. Examples of the respective heating courses are shown in figure 12.

Experiments with extracellular heating were carried out using suspensions in a volume of 1.8 ml containing 400 000 cells (suspended initially in 200 µl of culture medium) and LSMO(0.25)–SiO_2 nanoparticles at a concentration of $0.9\,mg_{Mn}\,ml^{-1}$. The suspensions were subjected to the AC magnetic field of $H_{max} = 6.4\,kA\,m^{-1}$ and $\nu = 481\,kHz$. The observed slow increase in the temperature (figure 12, curve *a*) can be ascribed primarily to the influence of thermal losses,

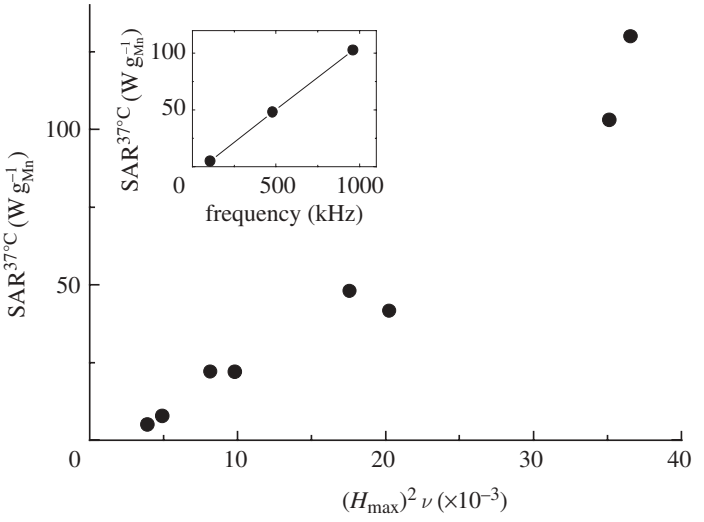

Figure 11. Dependence of SAR on the parameters of the applied alternating magnetic field. Inset—dependence of SAR on the frequency, $H_{max} = 6.07\,\mathrm{kA\,m^{-1}}$.

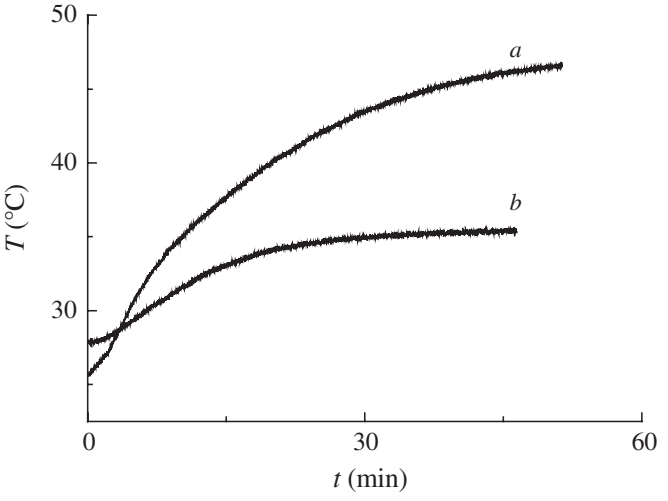

Figure 12. Magnetic heating: (*a*) extracellular; (*b*) intracellular.

which play the decisive role due to the relatively small content of magnetically active particles. Nevertheless, the influence on the heating efficiency as a result of a gradual decrease in the magnetization due to an increase in the temperature on approaching the Curie temperature should also be considered. Therefore, the required low terminal temperature of approximately 45°C was achieved.

Experiments with internalized nanoparticles were done solely on suspensions of cells (400 000 cells/200 µl medium) labelled in advance either by LSMO(0.25)–SiO_2 or by LSMO(0.25)–(SiO_2–NH_2–fluorescein–SiO_2) and subjected to the AC magnetic field of $H_{max} = 8.9\,\mathrm{kA\,m^{-1}}$ and $\nu = 481\,\mathrm{kHz}$. A small increase in the

Table 5. *In vitro* examinations.

	number of cells (thousands)	viability before the experiment (%)	viability after the experiment (%)
magnetic heating experiments			
extracellular heating: suspension of LSMO(0.25)–SiO_2 and cells	500	96	15
intracellular heating: suspension of cells containing internalized LSMO(0.25)–SiO_2	500	75	50
intracellular heating: suspension of cells containing internalized LSMO(0.25)–(SiO_2–NH_2–fluorescein–SiO_2)	500	85	75
blind experiments			
LSMO(0.25)–SiO_2 and cells, room temperature, 2 h	500	97	95
LSMO(0.25)–SiO_2 and cells, water bath, 35°C, 2 h	500	97	85
suspension of cells, no magnetic particles under magnetic field $H_{max} = 8.9\,kA\,m^{-1}$, $\nu = 481\,kHz$, 2 h	500	97	86

temperature from approximately 26°C up to approximately 34–35°C during the experiment can be attributed to a slight transfer of heat from the exciting coil and from the particles incorporated in the cells.

The results of *in vitro* examinations summarized in table 5 unambiguously show the effect of magnetic heating in contrast to the comparative blind experiments where no significant changes in the viabilities were observed.

The applied magnetic heating led to a substantial drop in the viabilities for the extracellular experiments, down to 10–20% from the initial values of approximately 96 per cent. Further, an important influence of the magnetically induced heating by particles incubated into the cells was discovered. Thus, a decrease in the viabilities from the initial values of approximately 75 per cent down to approximately 50 per cent just after the magnetic thermal treatment was detected in the samples containing cells labelled with LSMO(0.25)–SiO_2. A similar but less important effect was observed for samples containing cells labelled with LSMO(0.25)–(SiO_2–NH_2–fluorescein–SiO_2) nanoparticles, where the magnetic thermal treatment led to a decrease in the viabilities from approximately 85 to approximately 75 per cent.

After heat treatment, the cell morphology was changed—the cells were swollen when compared with cells in control samples and some of them had burst (figure 13). Since the distribution of nanoparticles inside the cells was not uniform, we believe that a certain number of nanoparticles are necessary to destroy the cell. Therefore, cells containing fewer nanoparticles were able to survive the heating process, and a decrease in the viability only to 50–75% was detected. An additional drop of 10–20% in the number of live cells overnight might probably be ascribed to an apoptosis initiated by the heating process.

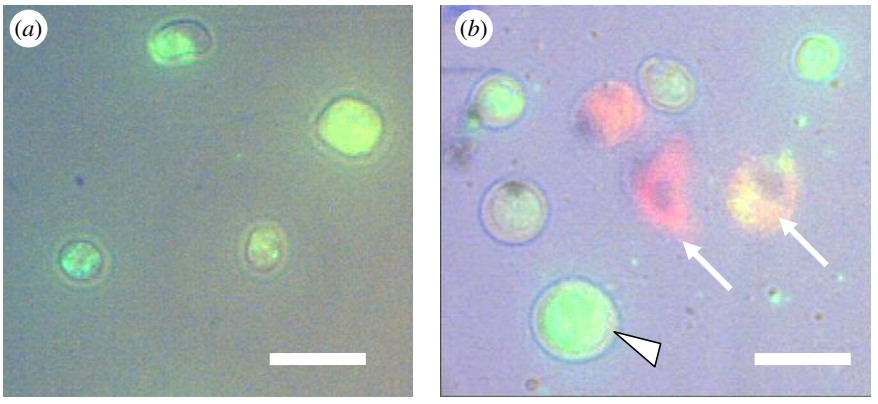

Figure 13. Rat MSCs labelled with fluorescein nanoparticles (*a*) before and (*b*) after the heating experiment during the trypan blue exclusion test. The overlay of fluorescent and light microscopy images shows intact cell membranes (dark circles around green cells). Cells after treatment are swollen (arrowhead) or have burst (arrows). Dead cells are in red. Scale bar, 20 µm.

7. Conclusion

Acid–base equilibria influencing the competing reactions during sol–gel processing, i.e. the formation of citric–metal complexes and simultaneous polyesterification, were suitably adjusted. Therefore, formation of a cross-linked polyester network occurs, where metal species and complexes become stabilized, their segregation is suppressed and compositional homogeneity is achieved.

Heating experiments carried out in AC magnetic fields with frequencies and amplitudes appropriate for future medical applications on stable water suspensions of LSMO(0.25)–SiO_2 with a concentration of $c_{Mn} = 3.39\,mg\,ml^{-1}$ revealed a maximum achieved temperature of $T_{max} = 64°C$ in rough correspondence with the determined Curie temperature. The highest specific absorption rate at 37°C, $SAR^{37°C}$, of $130\,W\,g_{Mn}^{-1}$ was reached for the applied $H_{max} = 8.7\,kA\,m^{-1}$ and $\nu = 480\,kHz$.

In vitro experiments were carried out in order to distinguish extracellular and intracellular magnetic heating effects. The extracellular heating experiments were done with LSMO(0.25)–SiO_2 nanoparticles at a concentration of $0.9\,mg_{Mn}\,ml^{-1}$. The maximum temperature during the experiments of approximately 45 min duration reached approximately 45°C. The applied magnetic heating led to a substantial drop in the viabilities, down to 10–20% from the initial values of approximately 96 per cent. The intracellular heating experiments were done on suspensions of cells labelled in advance either by LSMO(0.25)–SiO_2 or by LSMO(0.25)–(SiO_2–NH_2–fluorescein–SiO_2) in the contents of 0.17 and $0.18\,pg_{Mn}$/cell, respectively, measured by magnetic resonance imaging. Though the temperature of the liquid medium remained stable at approximately 34–35°C, a decrease in the viabilities of the cells from the initial values of approximately 75 per cent down to approximately 50 per cent for samples containing cells labelled by LSMO(0.25)–SiO_2 was observed. A much smaller effect in the same direction was observed for samples labelled with LSMO(0.25)–(SiO_2–NH_2–fluorescein–SiO_2) nanoparticles, where a decrease in

the cell viabilities from approximately 85 to approximately 75 per cent was found. Simultaneously, the use of fluorescein markers made it possible to directly observe some details of the changes of the cells due to magnetic heating by optical microscopy.

This study was performed under the support of the Academy of Sciences of the Czech Republic (KAN200200651 and KAN201110651) and EC-FP6-project DiMI, LSHB-CT-2005-512146.

One of the authors, E.P., would like to express his gratitude to Prof. M. Yoshimura for a helpful discussion concerning the mechanisms of the sol–gel processing during the Nanoparticles 2009 conference held in Liverpool.

References

Andrä, W. 1998 Magnetic hyperthermia. In *Magnetism in medicine* (eds W. Andrä & H. Nowak), p. 455. Weinheim, Germany: Wiley-VCH.

Arrot, A. 1957 Criterion for ferromagnetism from observations of magnetic isotherms. *Phys. Rev.* **108**, 1394–1396. (doi:10.1103/PhysRev.108.1394)

Asamitsu, A., Morimoto, Y., Kumai, R., Tomioka, Y. & Tokura, Y. 1996 Magnetostructural phase transitions in $La_{1-x}Sr_xMnO_3$ with controlled carrier density. *Phys. Rev. B* **54**, 1716–1723. (doi:10.1103/PhysRevB.54.1716)

Azizi, S. A., Stokes, D., Augelli, B. J., DiGirolamo, C. & Prockop, D. J. 1998 Engraftment and migration of human bone marrow stromal cells implanted in the brains of albino rats—similarities to astrocyte grafts. *Proc. Natl Acad. Sci. USA* **95**, 3908–3913. (doi:10.1073/pnas.95.7.3908)

Carvalho, K. A. *et al.* 2008 Evaluation of bone marrow mesenchymal stem cell standard cryopreservation procedure efficiency. *Transplant. Proc.* **40**, 839–841. (doi:10.1016/j.transproceed.2008.03.004)

Hergt, R., Hiergeist, R., Hilger, I. & Kaiser, W. A. 2002 Magnetic nanoparticles for thermoablation. *Recent Res. Dev. Mater. Sci.* **3**, 723–742.

Hill, D. A. 1985 Further studies of human whole-body radiofrequency absorption rates. *Bioelectromagnetics* **6**, 33–40. (doi:10.1002/bem.2250060104)

Jirák, Z., Hadová, E., Kaman, O., Kníek, K., Maryško, M., Pollert, E., Dlouhá, M. & Vratislav, S. 2010 Ferromagnetism versus charge ordering in the $Pr_{0.5}Ca_{0.5}MnO_3$ and $La_{0.5}Ca_{0.5}MnO_3$ nanocrystals. *Phys. Rev. B* **81**, 024403. (doi:10.1103/PhysRevB.81.024403)

Jordan, A. *et al.* 2001 Presentation of a new magnetic field therapy system for the treatment of human solid tumors with magnetic fluid hyperthermia. *J. Magn. Magn. Mater.* **225**, 118–126. (doi:10.1016/S0304-8853(00)01239-7)

Kačenka, M. *et al.* Submitted. Dual imaging probes for MRI and fluorescence microscopy based on manganite nanoparticles.

Kakihana, M. & Yoshimura, M. 1999 Synthesis and characteristics of complex multicomponent oxides prepared by polymer complex method. *Bull. Chem. Soc. Jpn.* **72**, 1427–1443. (doi:10.1246/bcsj.72.1427)

Kallumadil, M., Tada, M., Nakagawa, T., Abe, M., Southern, P. & Pankhurst, Q. A. 2009 Suitability of commercial colloids for magnetic hyperthermia. *J. Magn. Magn. Mater.* **321**, 1509–1513. (doi:10.1016/j.jmmm.2009.02.075)

Kaman, O. *et al.* 2009 Silica encapsulated manganese perovskite nanoparticles for magnetically induced hyperthermia without the risk of overheating. *Nanotechnology* **20**, 275610. (doi:10.1088/0957-4484/20/27/275610)

Lu, J. J., Deng, H. Y. & Huang, H. L. 2000 Thermal relaxation of interacting fine magnetic particles—field-cooled and zero-field-cooled magnetization variation. *J. Magn. Magn. Mater.* **209**, 37–41. (doi:10.1016/S0304-8853(99)00640-X)

Mornet, S., Vasseur, S., Grasset, F. & Duguet, E. 2004 Magnetic nanoparticle design for medical diagnosis and therapy. *J. Mater. Chem.* **14**, 2161–2175. (doi:10.1039/b402025a)

Mornet, S., Vasseur, S., Grasset, F., Veverka, P., Goglio, G., Demorgues, A., Portier, J., Pollert, E. & Duguet, E. 2006 Magnetic nanoparticle design for medical applications. *Prog. Solid State Chem.* **4**, 237–247. (doi:10.1016/j.progsolidstchem.2005.11.010)

Néel, L. 1949 Théorie du traînage magnétique des ferromagnétiques en grains fins avec application aux terres cuites. *Ann. Géophys.* **5**, 99–136.

Pankhurst, Q. A., Conolly, J., Jones, S. K. & Dobson, J. 2003 Applications of magnetic nanoparticles in biomedicine. *J. Phys. D Appl. Phys.* **36**, 167–181. (doi:10.1088/0022-3727/36/13/201)

Pankhurst, Q. A., Thanh, N. K. T., Jones, S. K. & Dobson, J. 2009 Progress in applications of magnetic nanoparticles in biomedicine. *J. Phys. D Appl. Phys.* **42**, 224001. (doi:10.1088/0022-3727/42/22/224001)

Papanastasiou, G. & Ziogas, I. 1989 Acid–base equilibria in binary water/organic solvent systems: dissociation of citric acid in water/dioxan and water/methanol solvent systems at 25°. *Talanta* **36**, 977–983. (doi:10.1016/0039-9140(89)80178-X)

Pollert, E., Kníek K., Maryško M., Kašpar P., Vasseur S. & Duguet E. 2007 New T_c-tuned magnetic nanoparticles for self-controlled hyperthermia. *J. Magn. Magn. Mater.* **316**, 122–125. (doi:10.1016/j.jmmm.2007.02.031)

Pollert, E., Veverka, P., Veverka, M., Kaman, O., Závěta, K., Vasseur, S., Epherre, R., Goglio, G. & Duguet, E. 2009 Search of new core materials for magnetic fluid hyperthermia: preliminary chemical and physical issues. *Prog. Solid State Chem.* **37**, 1–14. (doi:10.1016/j.progsolidstchem.2009.02.001)

Rosensweig, R. E. 2002 Heating magnetic fluid with alternating magnetic field. *J. Magn. Magn. Mater.* **252**, 370–374. (doi:10.1016/S0304-8853(02)00706-0)

Vasseur, S. *et al.* 2006 Lanthanum manganese perovskite nanoparticles as possible *in vivo* mediators for magnetic hyperthermia. *J. Magn. Magn. Mater.* **302**, 315–320. (doi:10.1016/j.jmmm.2005.09.026)

Závěta, K., Lančok, A., Maryško, M. & Pollert, E. 2006 Superparamagnetic properties of γ-Fe_2O_3 particles: Mössbauer spectroscopy and d.c. magnetic measurements. *Czech. J. Phys.* **56**, E83–E91. (doi:10.1007/s10582-006-0474-y)